A COMPUTATIONAL STUDY OF THE ADVANCING SIDE LIFT PHASE PROBLEM

R. Steijl, G. Barakos and K. Badcock
CFD Laboratory, Department of Aerospace Engineering, University of Glasgow, Glasgow G12 8QQ, U.K.
www.aero.gla.ac.uk/Research/CFD

Abstract

The numerical prediction of vibratory airloads and the corresponding structural response in high speed forward flight of helicopters pose a significant challenge to predictive methods, e.g. Refs.[1, 2]. Comparing of experimental data with results from predictive methods revealed two key discrepancies[2]: i) The phase prediction of advancing blade lift in high speed forward flight is predicted well ahead in azimuth when compared to measurements. ii) The prediction of the sectional pitching moment is poor, both in terms of phase and magnitude. Correlations of results from predictive methods and measured data (Army/NASA UH-60A Airloads Program[3]) for the advancing blade lift phase have improved significantly since the recent correction[4]. However, predicting the correct phasing is still a significant challenge, as is the prediction of the pitching moments. In the present work, the unsteady 3D flow field on the advancing side of a helicopter is analysed in an attempt to quantify the effects on the lift phase of the rotor trim state, blade normal Mach number variations and cross flow. It is shown that approximately 10^o of the phase delay can be attributed to the trim state of the helicopter. Time-dependent 2D CFD simulations of blade sections in pitch oscillation and combined pitch/free-stream Mach number oscillation show a phase delay in loading of approximately 10^o. Finally, CFD results for the UH-60A rotor in high-speed forward flight with constant blade pitch showed a phase delay of the advancing blade lift of around 25^o at the 77.5% radial station.

1 Introduction

The analysis of helicopter rotors is a challenging multidisciplinary problem, involving modeling of three-dimensional unsteady flow fields, transonic flows with moving shocks, reversed flow, separated flow, transition to turbulence, vortical wakes and modeling of the rigid-body motion of the rotor blades and their elastic deformation. A detailed account of all aerodynamic challenges related to the analysis of helicopter rotors is described in the review paper of Conlisk [5].

The flow conditions on the advancing and retreating side of rotors are quite different and rich in flow physics. On the advancing side, which is the target of this work, the blade normal Mach number is into the transonic regime with strong compressibility effects. The outboard part of the blade experiences large pitching moments and rapid pitching moment variations, which leads to high vibratory loads and high control loads for the blade pitch changes. Furthermore, the large pitching moments and their rapid variations can trigger strong torsional response of the blades. Helicopter rotor blades typically use aerodynamic sections with low pitching moments in steady aerodynamic conditions. The large pitching moments observed can be attributed to unsteady aerodynamic effects. To accurately predict the rotor loads in high-speed forward flight it is therefore essential to correctly model and understand the unsteady aerodynamic phenomena occurring on the advancing side of the rotor disk.

The comprehensive methods in use in rotorcraft research centers and the rotorcraft industry use lower-order aerodynamic models to obtain run times that allow routine use of these methods in design and analysis. Various level of structural modelling are in current use, ranging from modal to finite-element methods. The aerodynamic models in comprehensive methods usually involve lifting line models, indicial methods to model unsteady aerodynamics and/or table look-up methods for the sectional data. Indicial methods model the unsteadiness of the flow field. The rotor wake is modelled using a prescribed wake or a free-wake model.

Comprehensive methods based on these lower-order aerodynamic model have been found to give poor predictions in a number of situations. In the correlation of experimental data with results from predictive methods, two key discrepancies can be observed[2]: i) the phase prediction of advancing blade lift in high speed forward flight fail to predict the advancing blade phase delay and ii) the prediction of the section pitching moment is poor, both in phasing and magnitudes. The observations were made for different helicopters covering a range of different blade designs.

Fig 1(a) presents the sectional lift at 86.5% rotor radius for the UH-60A helicopter in high-speed forward flight for two thrust levels[6]. The peak of the negative lift at the outboard part of the blade on the advancing side occurs at around 120^o. The data from the Army/NASA UH-60A Airloads Program[3], using the recent correction[4], show a similar trend. Fig 1(b) compares the non-dimensional pitch-link loads for the swept-tip blade Puma and the UH-60A at similar advance ratios and thrust coefficients, highlighting the similarity of the loading at high advance ratio for the two different rotor designs.

Fig 2 presents a comparison of results obtained using the UMARC comprehensive analysis method and measured blade lift and pitching moments for the UH-60A helicopter at an advance ratio of 0.368. The figures show the sectional lift and pitching moment variation with blade azimuth typical for high-speed forward flight. The lift minimum on the advancing side (negative at outboard stations) occurs well aft of the $\psi = 90^o$ station. In this case, the delay is about 30^o using the correction[4]. The pitching moment shows the rapid change from a nose-up (positive) pitching moment at the aft part of the rotor disk to a strong nose-down pitching moment on the advancing side. The azimuth correction improves the phase correlation. At the 77.5% radial station, a phase difference of the pitching moments is still present. Furthermore, the experimental data shows larger (magnitudes) of the pitching moments at inboard stations.

To improve the predictive capabilities, comprehensive methods have been coupled to CFD solution methods for the Navier-Stokes or Euler equations. In this approach, the lower-order aerodynamic models are typically still used to obtain the sensitivities to control angles and blade motions. The CFD data are usually exchanged with the comprehensive method after completion of each rotor revolution in the CFD solution. This is commonly referred to as *loose coupling*[8, 9, 10]. At convergence to a trimmed state, the lower-order aerodynamics of the comprehensive method have been completely replaced by the CFD predictions. This approach has been successfully used by Datta et al.[9, 11, 12] to analysis the UH-60A in high-speed forward flight, Potsdam et al.[10] for the airloads prediction of the UH-60A in various speed regimes and Datta and Chopra[13] for the analysis of the dynamic stall loads on the UH-60A in high-altitude flight.

In contrast to the loose coupling approach, a *direct coupling* approach involves a coupling between the structural model the flow solver during each time steps. This more expensive approach was compared to the loose coupling approach by Altmikus et al.[8] for forward-flight cases of the ONERA 7A model rotor. It was found that both approaches give very similar results for the cases considered. The additional complexity of the direct coupling approach, therefore, does not give better pitching moment or torsional deflection predictions.

In the present work, the advancing side aerodynamics is studied, aiming to estimate the effect of: i) unsteadiness of the flow, resulting from the pitching motion and varying blade normal Mach number ii) effect of 3D cross-flow iii) effect of blade tip sweep and iv) the effect the trim state.

In this investigation, the rotor blade is assumed rigid, eliminating the, potentially, important effect of the structural response on the rotor loads.

2 Validation test cases

The CFD method used in the present study is described and validated elsewhere (Refs [14, 15]). Further validation for both hovering and forward-flying rotors also given in the next sections.

2.1 UH-60A model rotor in hover

The test case considered here, is a hovering 4-bladed UH-60A rotor at a thrust of $c_T/\sigma = 0.085$, with a collective of 10.47^o and a coning angle of 2.31^o (details are shown in Fig 3), following the description of Dindar et al.[16] for the non-linear twist distribution. Fig 5 presents a comparison of the computed chordwise c_p distribution with the experimental data of Lorber[17]. The inviscid CFD simulations (using single-blade periodic grids) were carried out using 3 mesh densities. The results obtained on all grids are in good agreement with the experimental data. The predictions near the tip show slight grid dependence as a result of the sensitivity of the blade pressure to the position and strength of the tip vortex of the preceding blade. Overall the results show that CFD simulations using the present multi-block meshes capture the flow features well, including those around the swept-back tip.

2.2 Non-lifting ONERA model rotors

This rotor is a modified Alouette helicopter tail rotor tested by ONERA [18, 19]. Two different rotor blade configurations are considered here, shown in Fig 4. One has a nearly straight leading edge and a 75 cm radius. The second configuration has 30^o leading edge sweep on the outer 15% and has a radius of 83.5 cm. The blades used here are different from the ONERA experiment in that the tapered root parts of the blades are removed. i.e. the blade up to 37% radius of the straight blade and 33% radius of the swept-tip blade. Both blades have symmetric NACA four-digit sections, varying in relative thickness from 17% at the root (37% radius of the straight blade and 33% radius of the swept-tip blade) to 9% at the tip. Both blades have a linear taper, the tip chord is 70% of the widest chord. The increased blade radius of the swept-tip blade was achieved by adding a 85 mm part of 14.5% relative thickness at 80% radius of the straight blade, i.e. between 71.9% and 82% radius of the swept-tip blade. The sweep starts at 85.7% radius, at which station the relative thickness is 13.5%. Based on the root chord, the rotor aspect ratio is 4.518 for the straight blade and 5.03 for the swept-tip blade.

Table 1 shows the conditions for the test cases considered in this work. Inviscid simulations were carried out using a step size in azimuthal direction of 0.25^o. Sensitivity analyses showed that this is sufficiently small to capture the unsteadiness of the flow. For validation purposes, the 2 cases at $\mu = 0.45$ are discussed in this section. For a radial station at 90% radius, Fig 6 shows a comparison of the computed and experimental chordwise pressure distribution for 5 azimuthal stations on the advancing side. For both blade configurations the correlation of the computed results and the experimental data is very good. For the swept-tip blade, the experimental data show more scatter, however, correlation with CFD is still favourable.

Table 1: Test cases for ONERA 2-bladed model rotor in forward flight.

case	blade	M_{tip}	μ	grid size	$\Delta\psi$
I	straight	0.625	0.50	2,000,000	0.25
II	straight	0.600	0.45	2,000,000	0.25
III	swept-tip	0.628	0.45	2,600,000	0.25

3 Advancing blade aerodynamics

3.1 Static blade section characteristics

Fig 7 presents the static airfoil characteristics of the SC1095 section. Lift and pitching moment coefficients for various Mach numbers are shown for a Reynolds number of $4 \cdot 10^6$. The $k-\omega$ turbulence model was used in the CFD simulations. The results for the SC1095 section shown here are consistent with those of Ref.[20].

The change of pitching moment with angle of attack provides an indication of the position of the aerodynamic center. For low subsonic Mach numbers the slope is close to zero, indicating that the aerodynamic center is close to the quarter-chord position. Increasing the Mach number leads to a forward shift of the aerodynamic center (the ratio $(dC_{m,c/4}/d\alpha)/(dC_l/d\alpha)$ increases) up to a Mach number of around 0.7. The pitching moment break occurs between Mach 0.7 and 0.8, with a corresponding movement of the aerodynamic center to well aft of the quarter-chord position. The movement of the aerodynamic center with a Mach number increase into the supercritical regime from a position forward of the quarter-chord to one well aft can be seen as one of the major contributions to the rapid change in pitching moment from a nose-up at rear of the rotor disk to a strong nose-down moment on the advancing side of the rotor disk. The other major contribution stems from the pitch rate of the blade.

The SC1095R8 airfoil section which is more cambered than the SC1095 section and, as a result, it has a smaller (i.e. larger negative) zero-lift angle and larger pitching moment magnitudes (about the quarter-chord) than the SC1095 section. Static results for the SC1095R8 airfoil section are not shown here, but are qualitatively very similar to those of the SC1095 section.

3.2 Pitching and Mach number variation

The unsteady aerodynamic conditions at the advancing side of a helicopter are modelled here using 2D unsteady airfoil simulations with oscillatory pitch and combined pitch/free-stream Mach number oscillations. The oscillatory pitch motion models the blade pitch variations during a rotor revolution. The oscillatory free-stream Mach number models the varying blade normal Mach number during the rotor revolution.

For a section at fraction r/R of the rotor radius, the blade normal Mach number depends on the azimuth ψ as

$$M_n(r/R,\psi) \quad = \quad M_{tip}\frac{r}{R}\big[1+\frac{\mu}{r/R}\sin\psi\big] \qquad (1)$$

where M_{tip} is the (hover) tip Mach number and μ the advance ratio of the rotor. This Mach number variation can be modelled in a two-dimensional airfoil simulation by rewriting Equation (1) as:

$$M_n(r/R,t) \quad = \quad \hat{M}_\infty\big[1+\lambda\sin(2k\tilde{t})\big] \qquad (2)$$

where $\hat{M}_\infty$ is the Mach number in the two-dimensional simulation, $\lambda = \mu/(r/R)$ the effective advance ratio of the section at station r/R. In Equation (2), ω is the rotation rate of the rotor. The reduced frequency k is defined as $k = \omega c/2U$, with c the airfoil chord, U the free-stream velocity and $\tilde{t}$ the dimensionless time. To model this Mach number variation, the two-dimensional airfoil

Table 2: Conditions at radial stations of UH-60A rotor blade, $M_{tip} = 0.628$, $\mu = 0.368$

station	77.5% radius	92.0% radius
section	SC1095R8	SC1095
$M_{tip} \cdot \frac{r}{R}$	0.487	0.578
λ	0.475	0.400
k	0.040	0.035
$M_{n,min}$	0.26	0.35
$M_{n,max}$	0.72	0.81

is translated as:

$$x_c(\tilde{t}) = x_{c,0} - \frac{\lambda}{2k}\left[1 - \cos(2k\tilde{t})\right] \quad (3)$$

$$\frac{dx_c}{d\tilde{t}} = -\lambda \sin(2k\tilde{t}) \quad (4)$$

where x_c is the airfoil reference point. The rotor cyclic pitch is modelled as a periodic pitch change of the airfoil:

$$\theta(\tilde{t}) = \theta_0 - \theta_{1s}\sin(2k\tilde{t}) - \theta_{1c}\cos(2k\tilde{t}) \quad (5)$$

Here, two representative stations along the UH-60A rotor blade are considered: the first one at 77.5% radius (where the blade has a SC1095R8 section) and the second at 92.0% radius (where the blade has a SC1095 section). For the high-speed forward flight considered here, i.e. with $M_{tip} = 0.628$ and $\mu = 0.368$, the radial stations are modelled in 2D as summarized in Table 2. Fig 8 presents the sectional normal force and pitching moment coefficients for both types of oscillatory motions and at two blade stations. For the oscillatory pitching motion, shown in Fig 8(a), a small (less than 10^o) phase delay of the normal force is observed, with the normal force curve lagging the pitch oscillation.

On the 'advancing side' ($0 < \omega t < 180^0$), the pitching moments increases to the maximum negative magnitude, while the blade normal force is reduced as a result of the reduced blade pitch. On the 'retreating side' ($180^o < \omega t < 360^0$), the pitching moments show the maximum nose-up (positive) conditions. Comparing this pitching moment behaviour with the static pitching moments shown in Fig 7, it follows that the unsteadiness of the flow is dominating the pitching moment behaviour.

The combined pitching and Mach number oscillation, shown in Fig 8(b), shows a phase delay of the sectional normal force on the advancing side of around 10^o. This delay is slightly larger in this case than for the oscillatory pitching motion in Fig 8(a). This can be attributed to the higher Mach numbers during that part of the cycle, which increase the impulsive delay. The increased Mach number on the advancing side leads to larger negative pitching moment magnitudes compared to the pitching motion at constant Mach number. It is interesting to note that shape of the pitching moment curve in Fig 8(b) shows a marked similarity with the pitching moment curve measured in high-speed forward flight conditions.

Another interesting feature of the result in Fig 8(b) is the negative normal force around the $\psi = 90^o$ azimuth. Since the blade incidence remains positive throughout the cycle and the cambered SC1095 and SC1095R8 sections have a negative zero-lift incidence, this negative normal force is an effect of the unsteadiness.

From the 2D unsteady simulations it can be concluded that the unsteady transonic conditions on the advancing side lead to a phase delay of the lift of around 10^o for the considered conditions. Furthermore, the pitching motion and the free-stream Mach number variation explain (partly) the pitching moment curve observed in flight conditions.

3.3 3D cross flow, inflow and tip effects

It is important to stress that the 2D unsteady simulations shown in the preceding section neglected many important effects present in the 3D rotor case: complex inflow field, finite-span effects of the blades, cross-flow effects, blade torsion. First, a non-lifting rotor in high-speed forward flight conditions is considered here. This allows the analysis of a number of 3D effects: cross-flow, finite-span ('tip relief') and tip-geometry effects.

In the non-lifting cases considered, unsteady 'circulatory' effects, i.e. effects originating from the delayed effects on the blade pressure from the time-dependent advected wake, are absent. Therefore, the unsteady aerodynamics on the non-lifting rotor can be used to study 'impulsive' effects only.

For the 2D unsteady airfoil results discussed in the preceding section, the varying lift (and therefore circulation) creates a time-dependent wake that advects the circulation changes. As such, this wake contains a 'history' of the circulation changes. The time-dependent effect of this wake on the flow around the section is the 'circulatory' effect. In addition to the circulatory effect, impulsive effects are also present in the 2D unsteady airfoil section results.

As in Section 2, the ONERA model rotor is considered, in this case at $\mu = 0.45$ and $\mu = 0.50$. Fig 9 shows the variation of chordwise c_p versus azimuth for the two blade geometries of the non-lifting ONERA model rotor. The conditions are given in Table 1. Results are shown for two radial stations, the first at 85% rotor radius and the second at 90% rotor radius.

Fig 9(a) and Fig 9(b) show the results at the two radial stations for the straight-tip blade at $\mu = 0.45$. The plots clearly show a hysteresis of the supersonic pocket and normal shock position with blade azimuth ψ, i.e. the pressure distributions at $\psi = 60^o$ and $\psi = 120^o$ are very different, despite the identical blade-normal Mach numbers. The station further outboard (90% rotor radius) experiences higher Mach numbers, leading to stronger shocks. The hysteresis can be regarded as a delayed response of the pressure distribution to Mach number variations. Since the cases are non-lifting, the delay is not caused by 'circulatory' effects.

Results for the straight-tip blade at $\mu = 0.50$ are shown in Fig 9(c) and 9(d), compared to the results at $\mu = 0.45$. The increased advance ratio and higher tip Mach number leads to the stronger normal shocks and shock positions further aft. Furthermore, the hysteresis in the pressure variation with azimuth is increased. For the 85% radial station, the normal shock forms at around $\psi = 60^o$, and is still present at $\psi = 150^o$.

The results for the swept-tip blade at $\mu = 0.45$ show stronger shocks than for the straight-tip blade at this advance ratio, which can be attributed to the higher tip Mach number. The relief of compressibility effects due to the tip-sweep does not fully compensate for this higher tip Mach number. Around $\psi = 90^o$, the tip-sweep clearly reduces the shock strength, but now a stronger shock occurs at larger blade azimuth ψ. The stronger hysteresis in the surface pressure distribution for the swept-tip blade can be explained from geometric considerations, since the tip sweep delays the maximum blade normal Mach numbers to larger values of ψ. The added phase shift relative to the straight-tip blade results is similar to the tip-sweep angle.

In the case of a lifting rotor, the situation is significantly more complicated due to the presence of a three-dimensional inflow field. Furthermore, 'circulatory' effects will be present along with the 'impulsive' effect analysed here.

Fig 10 presents results for the UH-60A rotor in forward flight. The tip Mach number is 0.628 and the advance ratio is 0.368. The CFD simulation was carried out using a fixed blade pitch of 5.0^o at 70% radius. Fig 10(a) shows the sectional normal force for the 77.5% and 92.0% radial stations. The fixed blade pitch creates a maximum sectional lift on the advancing side. However, this maximum occurs well aft of the $\psi = 90^o$ station where the maximum blade-normal Mach number is encountered. For the 77.5% radial station, this delay is 25^o. Further outboard, the delay is significantly smaller. The sectional pitching moments shown in Fig 10(b) shows the increased (negative) magnitudes on the advancing side. Since a blade pitching motion is

Table 3: Trim data for UH60 in high-speed forward flight [12].

	Flight test	CFD
μ	0.368	0.368
C_T/σ	0.0783	0.0783
α_s	6.98	7.67
θ_0	13.21	16.38
θ_{1s}	9.07	9.90
θ_{1c}	-6.56	-2.9

absent, this can be attributed to the aft movement of the aerodynamic center at super-critical Mach numbers. Fig 10(c) and Fig 10(d) show the integrated aerodynamic loads on the blades and, as can be seen, the delay in blade flapping moment corresponds to the phase delay in the sectional blade lift. The integrated blade pitching moment follows the sectional behaviour of Fig 10(b).

3.4 Rotor trim state

A typical rotor trim state involves: i) a forward rotor shaft tilt, that combined with the typically small lateral flapping β_{1c} leads to the required forward tilt of the rotor disk, ii) a positive θ_{1s} and negative θ_{1c}, which both increase in magnitude with increasing advance ratio of the rotor, and iii) flapping angles β_{1c}, β_{1c} that are typically (much) smaller in magnitude than the cyclic pitch angles. As a consequence of the trimming, most of the rotor load is carried by the front and aft part of the rotor disk and this increases with increasing advance ratio. At high advance ratios, the outer part of the rotor blade experiences negative lift in a section of the second quadrant ($90^o < \psi < 180^o$) on the advancing side of the rotor disk. For these blade azimuths, the inboard sections still create a small positive lift due to the twist in the blade. An example of a trim state for the UH-60A helicopter in high-speed forward flight is shown in Table 3. The blade geometric pitch (i.e. excluding the complex 3D inflow into the rotor disk), computed using the typical values for the blade harmonics and shaft tilt, shows a minimum blade incidence at around $\psi = 100^o$.

4 Conclusions

The present CFD investigation isolated separate aspects of the unsteady 3D transonic flow field, and its effect on the blade load phasing and pitching moments are quantified. 2D unsteady CFD results showed phase delays of around 10^o for lift for a pitching airfoil section in oscillatory free-stream Mach number conditions. CFD results for non-lifting rotors showed a distinct 'delayed' response to the changing Mach numbers. The results for the UH-60A rotor at constant blade pitch showed a phase delay of the advancing blade lift of around 25^o. Finally, it was shown that the trim state in high-speed conditions can add another 10^o in the blade lift delay.

Acknowledgements

The financial support of the Engineering Physical Sciences Research Council (EPSRC) and the UK Ministry of Defense (MoD) under the Joint Grant Scheme is gratefully acknowledged for this project. This work forms part of the Rotorcraft Aeromechanics Defense and Aerospace Research Partnership (DARP) funded jointly by EPSRC, MoD, DTI, QinetiQ and Westland Helicopters.

References

[1] Hansford, R. and Vorwald, J., Dynamics Workshop on rotor vibratory loads, American Helicopter Society 52nd Annual Forum, Washington D.C., June 4-6, 1996.

[2] Bousman, W., Putting the Aero Back Into Aeroelasticity, Eighth Annual ARO Workshop on Aeroelaticity of Rotorcraft Systems, University Park, PA, October 18-20, 1999.

[3] Kufeld, R., Balough, D., Cross, J., Studebaker, K., and Jennison, C., Flight Testing the UH-60A Airloads Aircraft. American Helicopter Society 50th Annual Forum, Washington D.C., May 11-13, 1994.

[4] Kufeld, R. and Bousman, W., UH-60A airloads program azimuth reference correction, *J. American Helicopter Society*, Vol. 50, No. 2, 2005, pp. 211–213.

[5] Conlisk, A., Modern helicopter aerodynamics, *Annual Review of Fluid Mechanics*, Vol. 29, 1997, pp. 515–567.

[6] Coleman, C. and Bousman, W., Aerodynamic Limitations of the UH-60A Rotor, Tech. Rep. TM-110396, NASA, 1996.

[7] Maier, T. and Bousman, W., An Examination of the Aerodynamic Moment on Rotor Blade Tips Using Flight Test Data and Analysis, Tech. Rep. TM-104006, NASA, 1993.

[8] Altmikus, A., Wagner, S., Beaumier, P., , and Servera, G., A Comparison: Weak versus Strong Modular Coupling for Trimmed Aeroelastic Rotor Simulations, American Helicopter Society 58th Annual Forum, Montreal, Quebec, June, 2002.

[9] Datta, A. and Chopra, I., Validation of structural and aerodynamic modeling using UH-60A flight test data, American Helicopter Society 59th Annual Forum, Phoenix, May 6-8, 2003.

[10] Potsdam, M., Yeo, H., and Johnson, W., Rotor Airloads Prediction Using Loose Aerodynamic/Structural Coupling, American Helicopter Society 60th Annual Forum, Baltimore, MD, June 7-10, 2004.

[11] Datta, A. and Chopra, I., Validation of structural and aerodynamic modeling using UH-60A flight test data. *J. American Helicopter Society*, Vol. 49, No. 3, 2004, pp. 271–287.

[12] Datta, A., Sitaraman, J., Chopra, I., and Baeder, J., Analysis Refinements for Prediction of Rotor Vibratory Loads in High-Speed Forward Flight, American Helicopter Society 60th Annual Forum, Baltimore, MD, June 7-10, 2004.

[13] Datta, A. and Chopra, I., Prediction of UH-60A Dynamic Stall Loads in High Altitude Level Flight using CFD/CSD Coupling, American Helicopter Society 61st Annual Forum, Grapevine, TX, June 1-3, 2005.

[14] Badcock, K., Richards, B., and Woodgate, M., Elements of Computational Fluid Dynamics on Block Structured Grids Using Implicit Solvers, *Progress in Aerospace Sciences*, Vol. 36, 2000, pp. 351–392.

[15] Steijl, R., Barakos, G., and Badcock, K., A Framework for CFD Analysis of Helicopter Rotors in Hover and Forward Flight, accepted for publication in Int. J. Num. Meth. Fluids, August 2005.

[16] Dindar, M., Shephard, M., Flaherty, J., and Jansen, K., Adaptive CFD analysis for rotorcraft aerodynamics. *Comput. Methods Appl. Mech. Engrg.*, Vol. 89, 2000, pp. 1055–1076.

[17] Lorber, P., Aerodynamic Results of a Pressure-Instrumented Model Rotor Test at the DNW, *J. American Helicopter Society*, Vol. 36, No. 4, 1991, pp. 66–76.

[18] Philippe, J.-J. and Chattot, J.-J., Experimental and theoretical studies on helicopter blade tips at ONERA, Sixth European Rotorcraft and Powered Lift Aircraft Forum, Bristol, September 16-19, 1980.

[19] Tauber, M., Chang, I., Caughey, D., and Philippe, J.-J., Comparison of Calculated and Measured Pressures on Straight- and Swept-Tip Model Rotor Blades, Tech. Rep. TM-85872, NASA, 1985.

[20] Smith, M., Wong, T., Potsdam, M., Baeder, J., and Phanse, S., Evaluation of CFD to Determine Two-Dimensional Airfoil Characteristics for Rotorcraft Applications, American Helicopter Society 60th Annual Forum, Baltimore, MD, June 7-10, 2004.

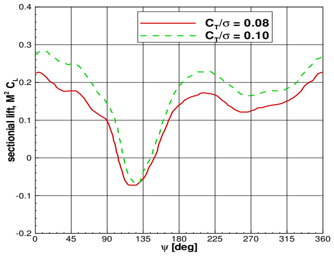

(a) Sectional lift (UH-60A, $r/R = 0.865$) $\mu = 0.37$, $C_T/\sigma = 0.08$, and $C_T/\sigma = 0.10$. Data scanned from Ref.[6].

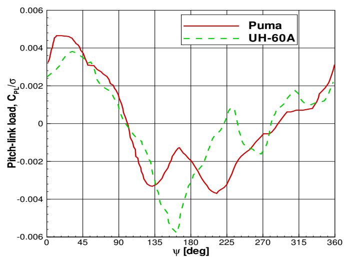

(b) Pitch-link load, Puma: $\mu = 0.362$, $C_T/\sigma = 0.07$ and UH-60A: $\mu = 0.355$, $C_T/\sigma = 0.08$. Data scanned from Ref.[7].

Figure 1: Sectional lift (a) and Pitch-link load (b) from flight test data.

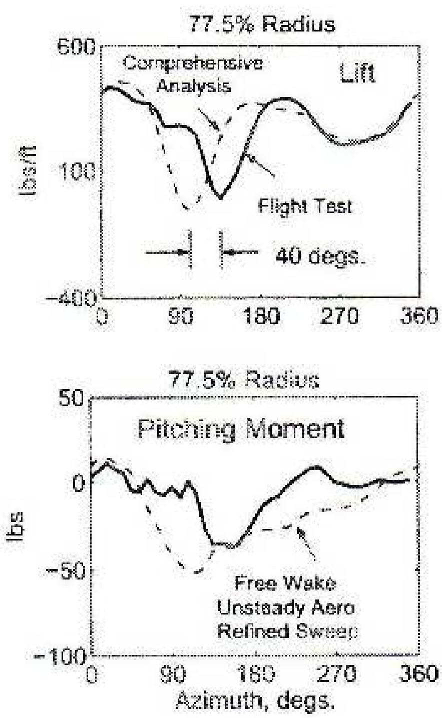

Figure 2: Comparison of computed (UMARC comprehensive method) and measured blade lift and pitching moments. UH-60A in high-speed forward flight, $\mu = 0.368$. Reproduced from [9].

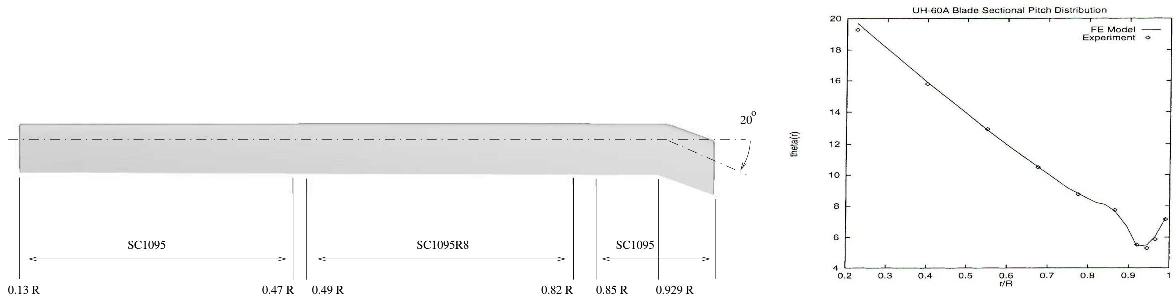

Figure 3: Geometry of UH-60A rotor blade. Non-linear twist according to Ref.[16].

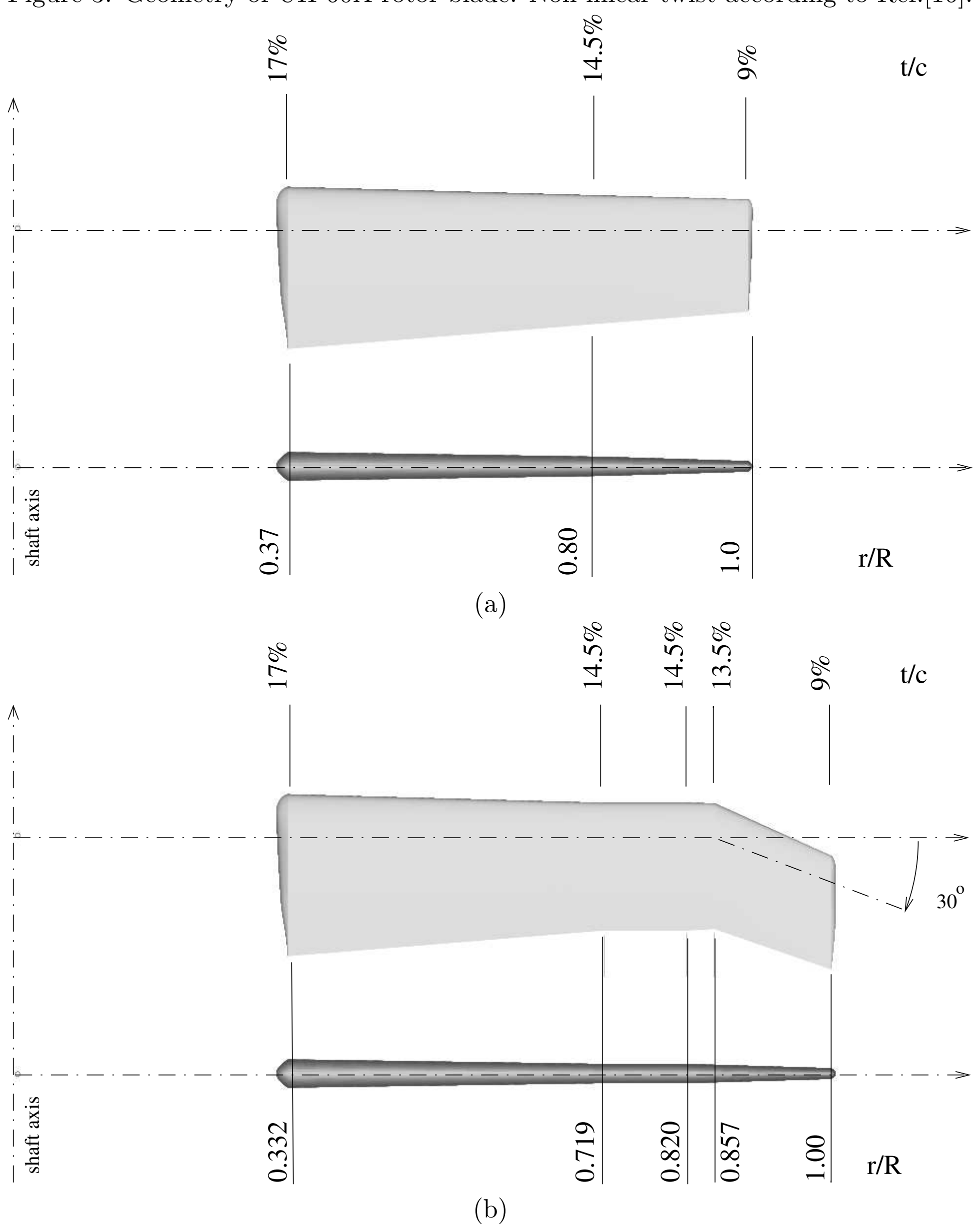

Figure 4: Geometry of non-lifting ONERA model rotor[18]: (a) straight blade (b) swept-tip blade.

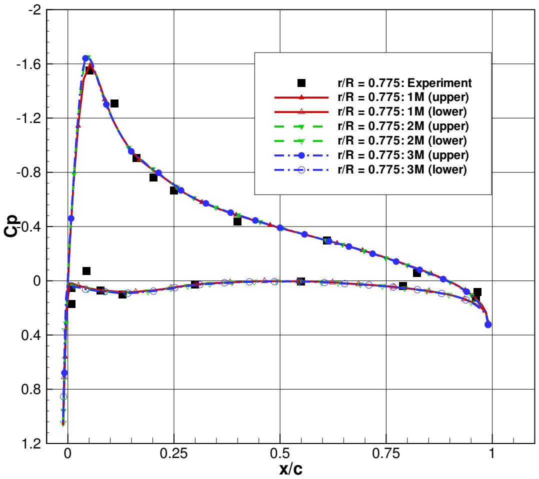

r/R=0.775

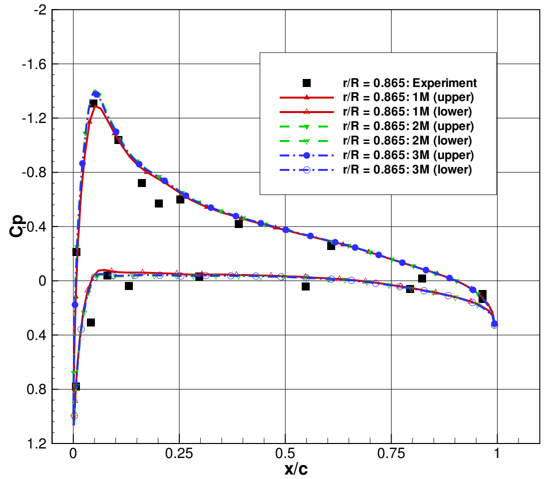

r/R=0.865

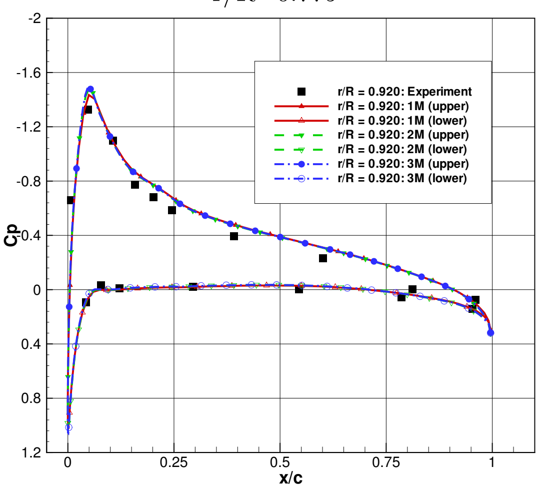

r/R=0.920

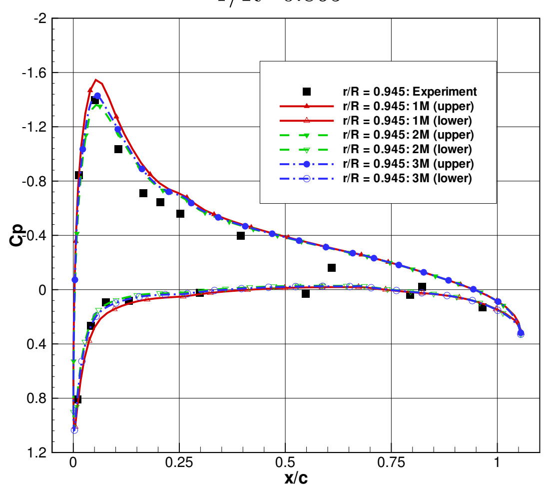

r/R=0.945

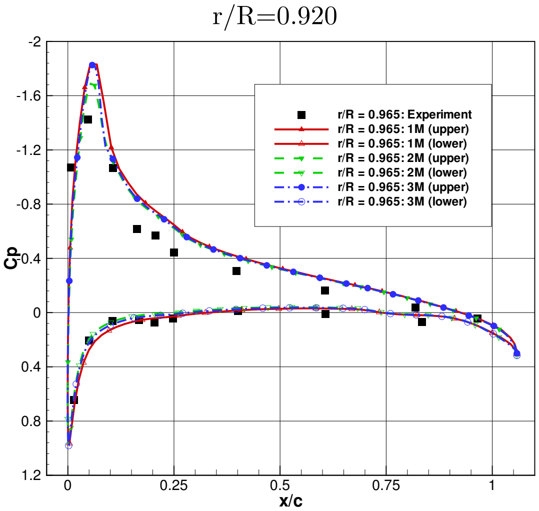

r/R=0.965

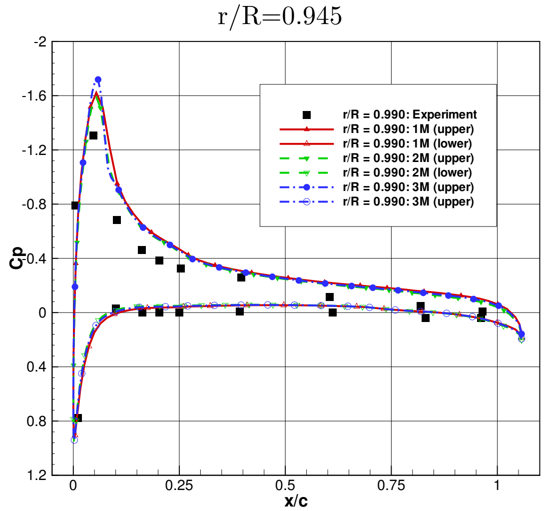

r/R=0.990

Figure 5: UH60A rotor in hover: $M_{tip} = 0.628$, 10.47^o collective, 2.31^o coning.

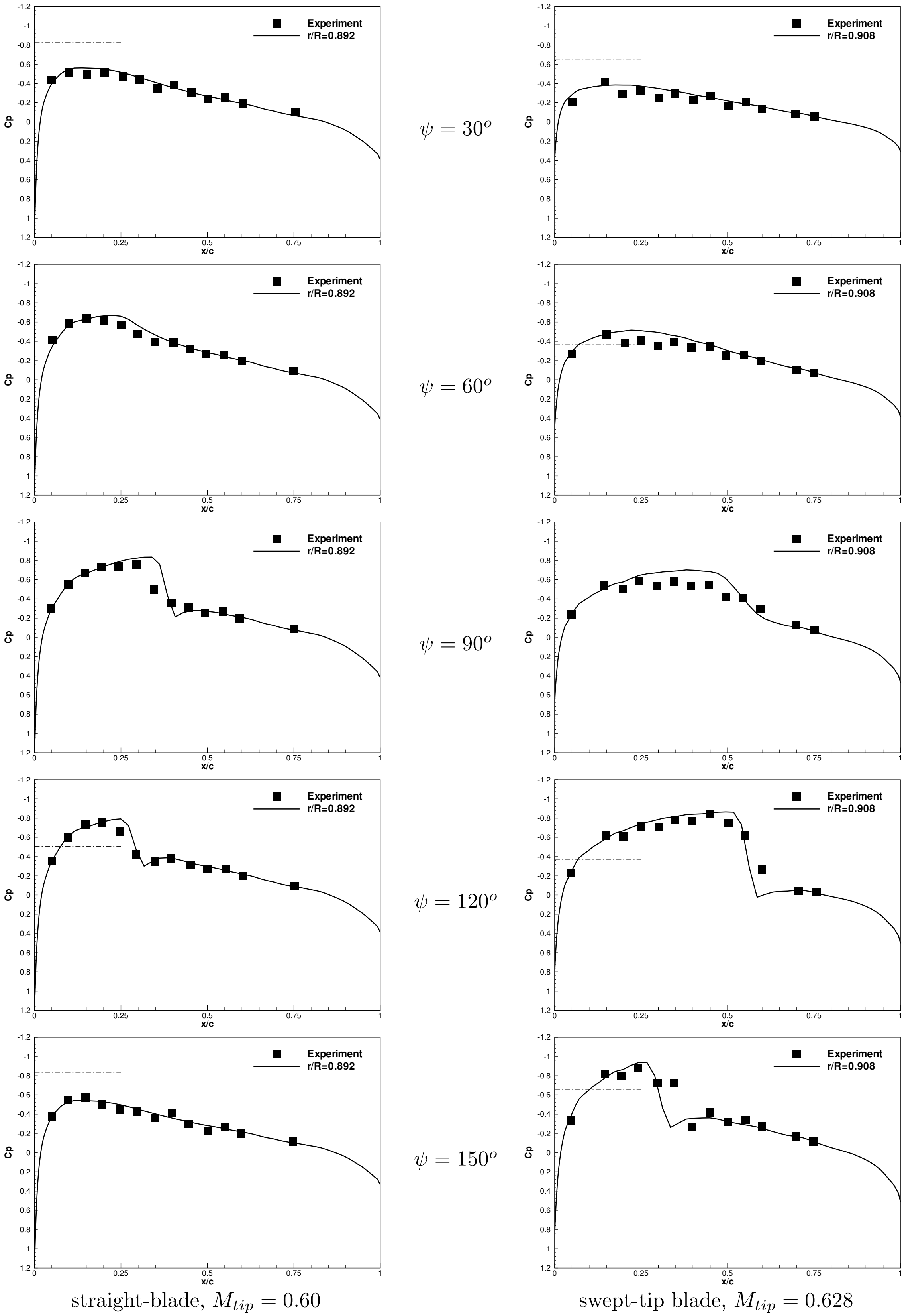

Figure 6: Validation test cases: comparison of computed chordwise c_p distribution with experiment. Non-lifting 2-bladed ONERA model rotor[18]. Straight-blade and swept-tip blade, $\mu = 0.45$.

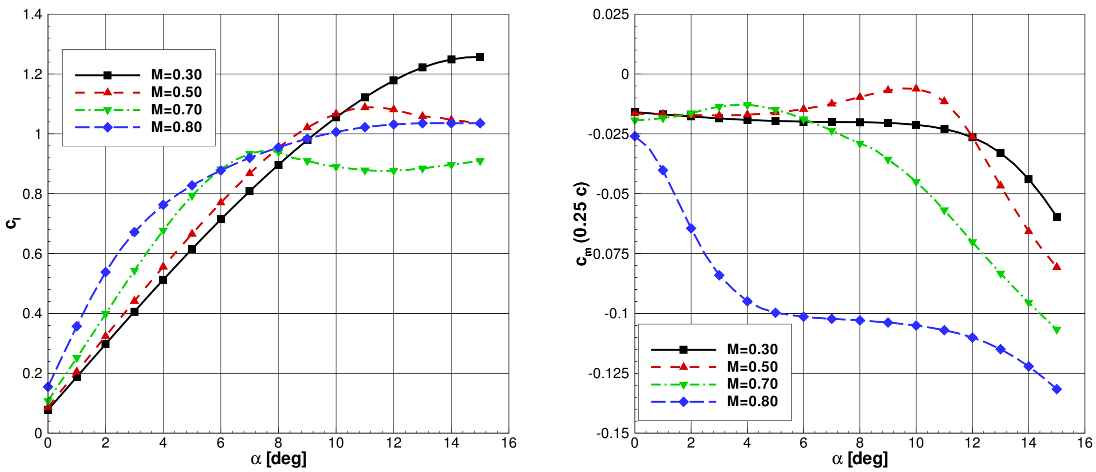

Figure 7: Static lift and pitching moment coefficient for SC1095 section, $Re = 4 \cdot 10^6$, $k - \omega$ turbulence model.

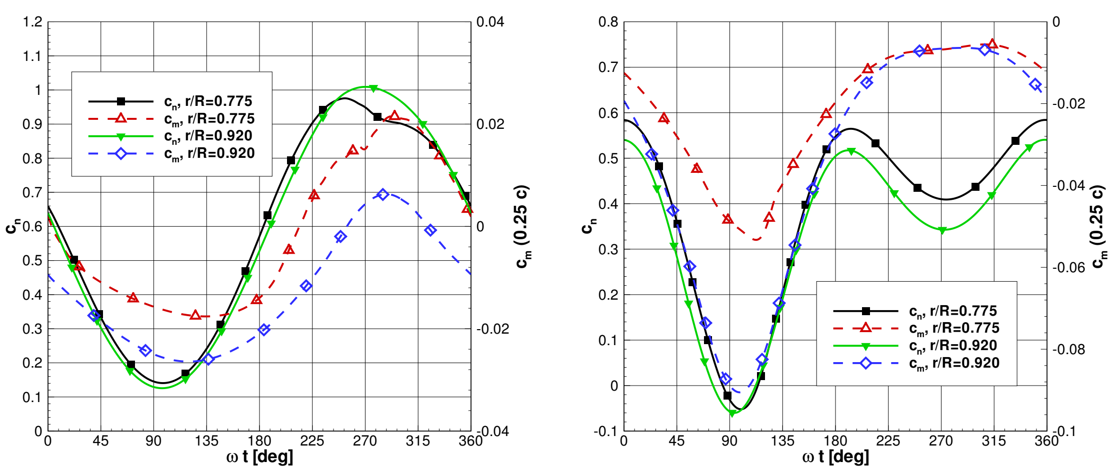

(a) (b)

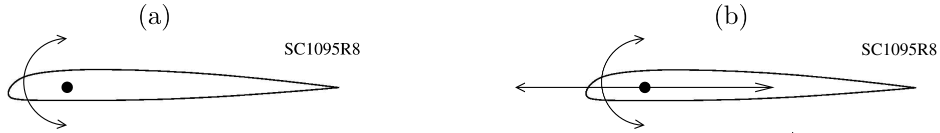

Pitch oscillation: $\alpha = 4^o - 4^o \sin \omega t$

Free-stream Mach number/pitch oscillation: $\alpha = 4^o - 4^o \sin \omega t$, $M = M_\infty(1 + \lambda \sin \omega t)$

Figure 8: Sectional normal force and pitching moment coefficient for SC1095R8 section ($M_\infty = 0.487$, r/R=0.775, k=0.04) and SC1095 section ($M_\infty = 0.578$, r/R=0.920, k=0.035). (a) Pitch oscillation and (b) combined free-stream Mach number/pitch oscillation. $Re = 4 \cdot 10^6$, $k - \omega$ turbulence model.

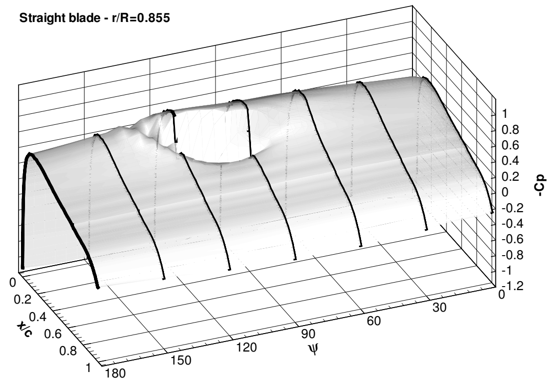

(a) Straight-tip: $M_{tip} = 0.60$, $\mu = 0.45$

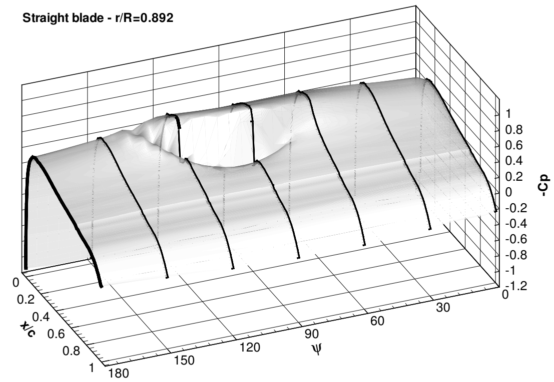

(b) Straight-tip: $M_{tip} = 0.60$, $\mu = 0.45$

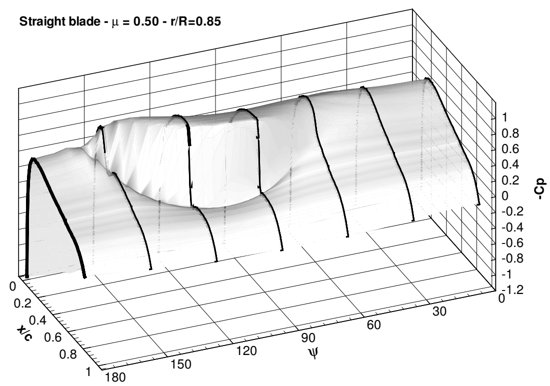

(c) Straight-tip: $M_{tip} = 0.625$, $\mu = 0.50$

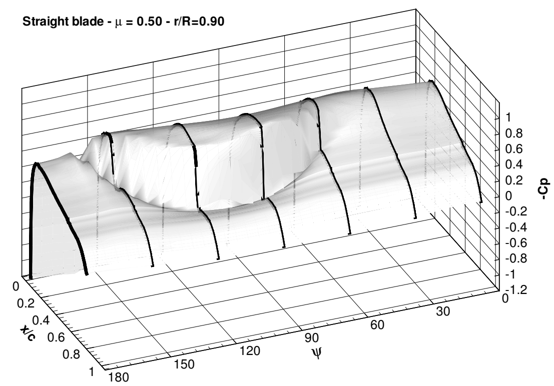

(d) Straight-tip: $M_{tip} = 0.625$, $\mu = 0.50$

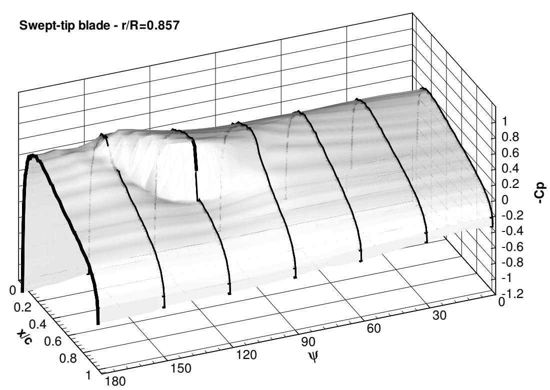

(e) Swept-tip: $M_{tip} = 0.628$, $\mu = 0.45$

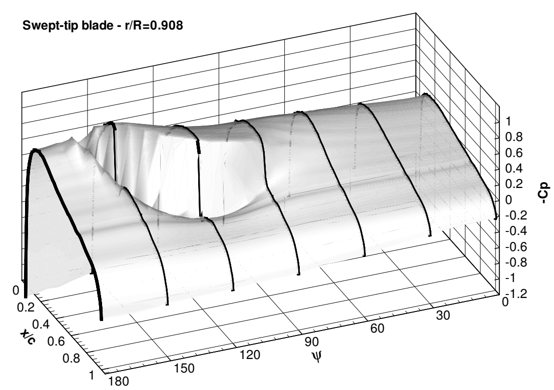

(f) Swept-tip: $M_{tip} = 0.628$, $\mu = 0.45$

Figure 9: Chordwise c_p versus azimuth for non-lifting ONERA model rotor, straight-tip and swept-tip blade configurations.

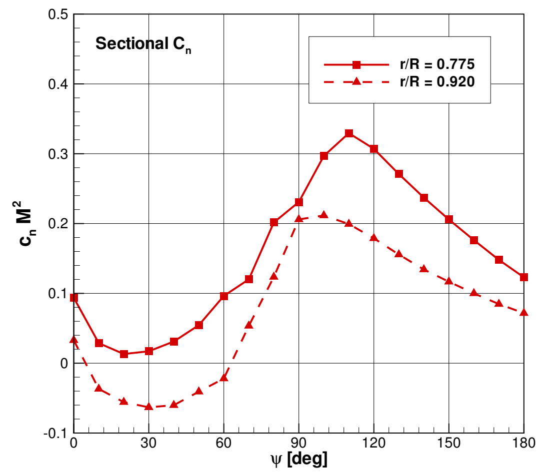

(a) Sectional c_n

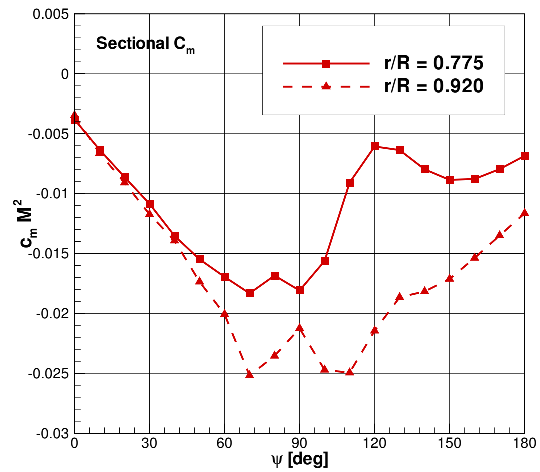

(b) Sectional c_m

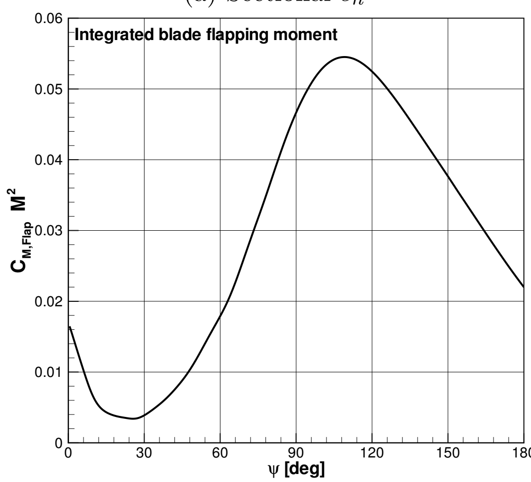

(c) Blade flapping moment (integrated airloads)

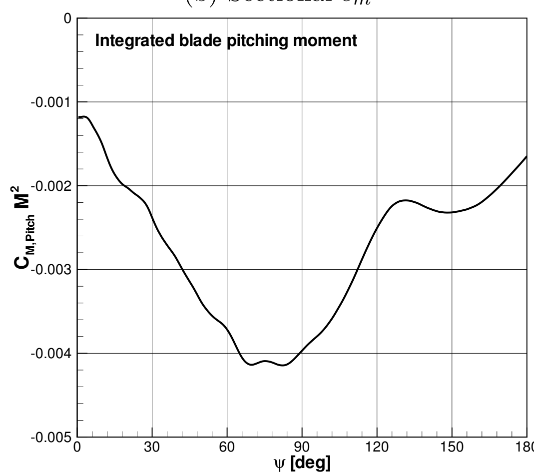

(d) Blade pitching moment (integrated airloads)

Figure 10: Results for UH-60A rotor in high-speed forward flight with constant blade pitch. $\mu = 0.368$, collective 5^o.